Geomechanics and Engineering, *Vol. 33, No. 4 (2023) 327-339*
https://doi.org/10.12989/gae.2023.33.4.327

Expansion performance and mechanical properties of expansive grout under different curing pressures

Yiming Liu[1a], Yicheng Ye[1,2b], Nan Yao*[1,2] and Changzhao Chen[1c]

[1]*School of Resources and Environmental Engineering, Wuhan University of Science and Technology, Wuhan 430081, China*
[2]*Hubei Key Laboratory for Efficient Utilization and Agglomeration of Metallurgic Mineral Resources, Wuhan, China*

(*Received May 11, 2021, Revised March 2, 2023, Accepted March 5, 2023*)

Abstract. The expansion capacity and strength of expansive grout have a significant influence on the stress state of a supported rock mass and the strength of a grout–rock mass structure. The expansion and strength characteristics are vital in grouting preparation and application. To analyze the expansion performance and mechanical properties of expansive grout, uniaxial compressive strength (UCS) tests, expansion ratio tests, XRD, SEM, and microscopic scanning tests (MSTs) of expansive grout under different curing pressure conditions were conducted. The microevolution was analyzed by combining the failure characteristics, XRD patterns, SEM images, and surface morphologies of the specimens. The experimental results show that: (1) The final expansion ratio of the expansive grout was linear with increasing expansion agent content and nonlinear with increasing curing pressure. (2) The strength of the expansive grout was positively correlated with curing pressure and negatively correlated with expansion agent content. (3) The expansion of expansive grout was related mainly to the development of calcium hydroxide ($Ca(OH)_2$) crystals. With an increase in expansion agent content, the final expansion ratio increased, but the expansion rate decreased. With an increase in the curing pressure, the grout expansion effect decreased significantly. (4) The proportion of the concave surfaces at the centre of the specimen cross-section reflected the specimen's porosity to a certain extent, which was linear with increasing expansion agent content and curing pressure.

Keywords: expansion evolution; expansive grout; failure characteristics; grouting reinforcement; uniaxial compressive strength mechanical properties

1. Introduction

Grouting reinforcement technology is widely used in underground engineering support for fractured rock masses (Saeidi *et al*. 2013, Wang *et al*. 2019). By grouting into rock mass fractures, the friction force and cohesive force of the fracture surfaces can be increased significantly improving the overall strength and stability of the fractured rock mass (Widmann 1996, Varol *et al*. 2006, EI Tani 2012).

With the widespread application of grouting reinforcement in underground geotechnical support, research has been widely developed on grouting materials and the mechanical changes of rock masses after grouting (Zhang *et al*. 2019) such as diffusion (Pedrotti *et al*. 2017), strength (Moayed *et al*. 2019), impermeability (Li *et al*. 2020), fatigue damage (Zhi *et al*. 2018), and the effects of grout (Shimada 2014, Liu *et al*. 2000). The limitations of traditional grouting materials are presented as follows: Portland cement is the primary cementitious material in grouting, which can provide only a bonding effect in the surrounding rock cracks. Portland cement undergoes dry shrinkage after its solidification (Lai *et al*. 2020), which may affect the bonding ability of the grout thus, referring to the support idea of split-set bolts providing circumferential prestress in rock masses by extruding rock in circumferential directions (Zhang 2020, Liu *et al*. 2020, Das 2020), adding an appropriate amount of expansion agent to the grout is proposed to squeeze the rock mass on both sides of the fractured surfaces. The grouting support for rock masses is improved in a three-dimensional stress state.

Expansion agents are mainly used in geotechnical engineering to compensate for concrete shrinkage caused by temperature stress (Huang *et al*. 2019) as well as providing intense expansion pressure (greater than 100 MPa) to fracture the rock mass (Shang *et al*. 2018a, Shang *et al*. 2018b). High-efficiency soundless crush agents (HSCAs), composed mainly of calcium oxide (CaO), are widely used in rock fracturing and concrete structure demolition (De Silva 2019, Natanzi *et al*. 2020, Laefer 2018). The basic principle of its expansion (De Silva *et al*. 2017) is that, the CaO reacts with water to form calcium hydroxide $Ca(OH)_2$ crystals, resulting in a solid volume expansion of approximately 97% of $Ca(OH)_2$ greater than the volume of CaO. When HSCA is injected into a borehole, the volume expansion squeezes the rock or the concrete which causes it to fracture by providing strong expansion stress.

The expansion capacity and strength of expansive grout

*Corresponding author, Associate Professor
E-mail: yaonan@wust.edu.cn
[a]M.Sc. Student
E-mail: liuyiming.wust@qq.com
[b]Professor
E-mail: yeyicheng@wust.edu.cn
[c]M.Sc. Student
E-mail: 18672507100@163.com

ISSN: 2005-307X (Print), 2092-6219 (Online)

Table 1 Chemical composition of grout materials w(%)

Materials	CaO	SiO_2	SO_3	Fe_2O_3	Al_2O_3	MgO	K_2O	TiO_2	Na_2O
42.5 # Portland cement	44.00	30.12	2.05	2.05	11.66	4.74	1.07	0.29	1.73
HSCA	87.12	4.47	0.04	2.76	2.78	0.75	0.06	0.09	0.21

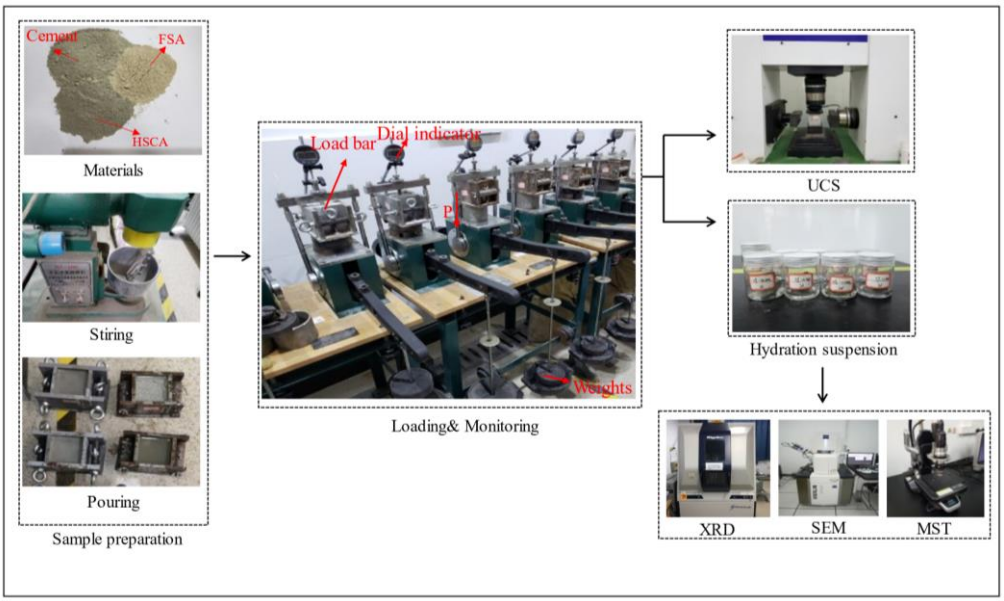

Fig. 1 Schematic of the experimental procedure

are important parameters that directly determine the application potential of grouting reinforcement. If the volume expansion of the grout is small, the supported rock mass is not in a three-dimensional state. If the volume expansion of the grout is large, it may directly fracture the rock mass and cause a secondary failure. The expansion evolution law of expansive grout and the influences of expansion performance based on cement and expansion agent contents (Yao *et al*. 2021) have been studied, but few studies barely focus on its strength. If the grout is too weak, the bearing capacity of the grout–rock structure becomes poor. In addition, in underground geotechnical engineering, the expansion behavior and strength of expansive grout are different under different in situ constraints stress, they are of great significance in expansive grout preparation and application under different curing pressures.

To analyze the expansion performance and mechanical properties of expansive grout under different curing pressure conditions, expansion ratio tests, UCS tests, XRD, SEM, and microscopic scanning tests (MSTs) were conducted. The macroscopic expansion performance and mechanical properties of the expansive grout were analyzed, including the volume expansion, UCS and failure characteristics, aided by microevolution analysis from XRD patterns, SEM images, and surface morphology.

2. Experiment

2.1 Materials

Table 2 Purification ratio

Water–cement ratio	Expansion agent (%)	FSA (%)	Defoaming agent (%)
0.7:1	0, 5, 10, 15, 20	0.25	0.1

The chemical composition of the raw materials used in the test includes; Huaxin 42.5 # Portland cement and HSCA, they were analyzed by x-ray fluorescence spectrometry (XRF), as shown in Table 1.

2.2 Proportion scheme

According to previous experiments, the water–cement ratio was set as 0.7:1 (Yao *et al*. 2021), and the expansion agent contents were set to 0%, 5%, 10%, 15%, and 20%. Minimal amounts of flash setting admixture (FSA) and defoaming agent were added to increase the cementation speed and reduce the air bubbles in the grout, respectively.

The 20°C clean tap water was used as the mixing water. The proportions are shown in Table 2.

2.3 Experimental procedure

The experimental procedure includes specimen preparation and treatment, expansion ratio tests, UCS tests, XRD, SEM, and MST. The experimental schematic is shown in Fig. 1.

2.3.1 Specimen preparation

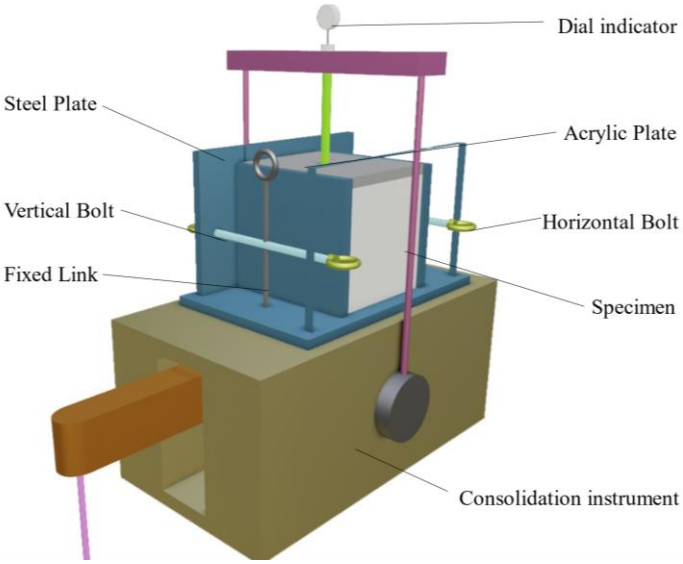

Fig. 2 Schematic of expansion monitoring

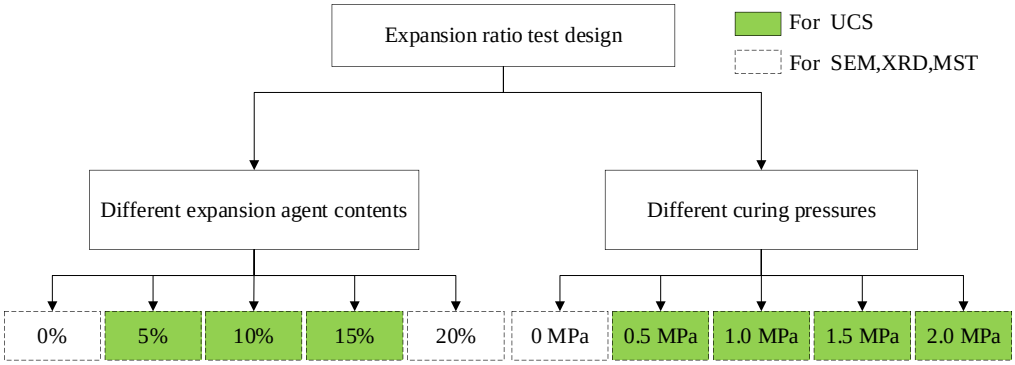

Fig. 3 Schematic of the Expansion ratio, UCS, SEM, XRD, and MST test design

The cement, HSCA, FSA, water, and defoaming agent were mixed according to the proportions in Table 2. After stirring, the mixture was poured into a steel mould with a square bottom surface with side length dimensions of 70.7 mm × 70.7 mm and a height of 85 mm. The height of the actual specimen in the mould was 70.7 mm, and the extra height was reserved for the grout expansion. The specimens were cured for seven days at a standard room temperature of 20°C. The data of the following experiments were taken on the seventh day, as the cement specimen's expansion did not generally change anymore after seven days period.

2.3.2 Expansion ratio test

In this test, the specimens began to undergo curing pressures after the final setting, approximately eight hours after their preparation. The curing pressures were 0 MPa, 0.5 MPa, 1.0 MPa, 1.5 MPa, and 2.0 MPa; 0 MPa representing no curing pressure. The other gradients of curing pressures were loaded in a consolidation instruments. A schematic of the expansion monitoring is shown in Fig. 2. A dial indicator was used to monitor the volume expansion. The final expansion ratios of the specimens were calculated using Eq. (1). The design of the expansion ratio test is shown in Fig. 3.

$$\varphi = \frac{L}{h_0} \times 100\% \tag{1}$$

Where L is the final height of the specimens (mm), and h_0 represents the initial height of 70.7 mm.

2.3.3 UCS test

Uniaxial compression tests were performed on some of the expansion test specimens. The strength of the specimens with different expansion agent contents (5%, 10%, 15%) and different curing pressures (0.5 MPa, 1.0 MPa, 1.5 MPa, 2.0 MPa) was tested using a YZW-30A uniaxial compressor. Three specimens were made for each condition and average values were taken to ensure the accuracy of the results. The failure characteristics were observed and analyzed. The specific test scheme is presented in Fig. 3.

2.3.4 XRD, SEM, and MST

To explore the microevolution process of expansive grout with different expansion agent contents and curing pressures, different expansion agent contents were set under a 1.0 MPa curing pressure, and different curing pressures were placed under 10% expansion agent content.

Specimens for XRD and SEM were ground into small

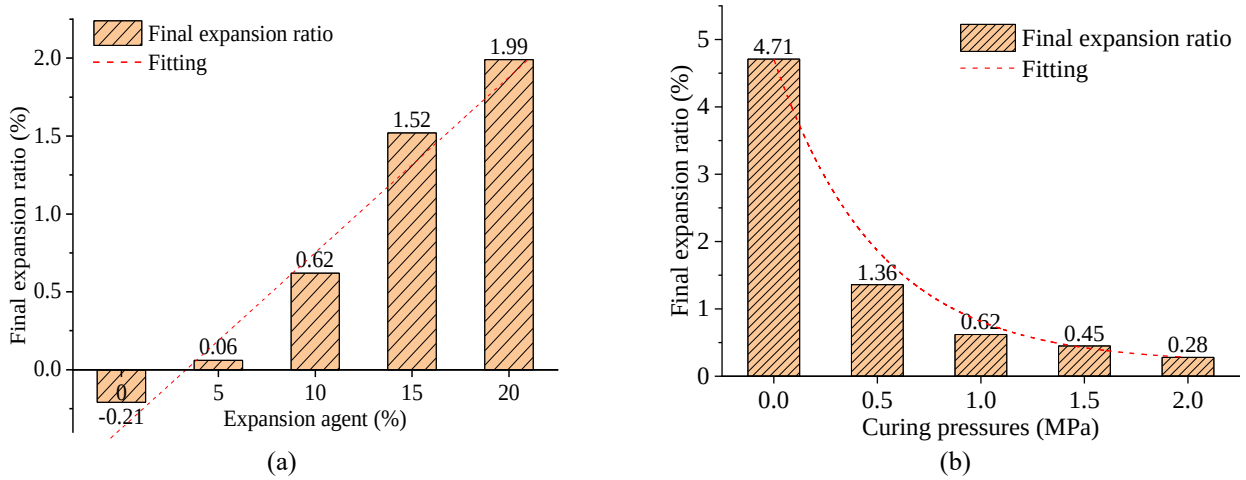

Fig. 4 Final expansion ratios of specimens under different conditions, (a) Different expansion agent contents (1.0 MPa) and (b) Different curing pressures (10%)

pieces with smooth edges and immersed in 21 mm-wide plastic bottles containing anhydrous ethanol to stop the hydration of the cement. The specimens were dried in a dryer for 1h purposely to remove moisture, some were ground into powder before the test. The expansive grout's chemical composition and microcrystal morphology were observed using a Smartlab 3 kW x-ray diffraction and FEI Talos F200 high-resolution transmission electron microscope.

Specimens for MST were cut from the center point using a metallographic specimen cutting machine, and the internal surface of the specimen was observed using a vhx-5000 ultra-depth of field digital micro scanner with 200 × magnification to obtain the characteristic parameters of surface morphology. The specific test scheme is presented in Fig. 3.

3. Expansion performance

The volume expansion ratio test results with different expansion agent contents (curing pressure 1.0 MPa) and different curing pressures (expansion agent content 10%) are shown in Fig. 4.

3.1 Different expansion agent contents

Under the same curing pressure condition (1.0 MPa), the expansion ratios of the specimens with different expansion agent contents are shown in Fig. 4(a). The final expansion ratio of the specimen was linear with increasing expansion agent content. When there was no expansion agent in the specimen, it gradually lost water and dry, leading to final volume contraction. The expansion agent can effectively compensate for the volume shrinkage of the grout under the action of curing pressure and hydration (Wang *et al*. 2014).

The final expansion ratios of the specimens were -0.21%, 0.06%, 0.62%, 1.52%, and 1.99% when the expansion agent contents were 0%, 5%, 10%, 15%, and 20%, respectively. With different expansion agent contents, the functional relationship between the final expansion ratio ρ and the expansion agent content φ (Fig. 4(a)) is expressed as

$$\rho = 0.117\varphi - 0.376, \quad R^2 = 0.962 \tag{2}$$

3.2 Different curing pressures

With the same expansion agent content (10%), the expansion ratio of the specimen under different curing pressures is shown in Fig. 4(b). The final expansion ratio of the specimen was nonlinear with increasing curing pressure, and the results with a curing pressure and no curing pressure were significantly different. When the applied curing pressure was low (0.5 MPa), the expansion of the specimen was significantly less than without an applied curing pressure, and there was little residual expansion.

When the curing pressure was moderate (1.0 MPa), the grout expansion and development time was 24 h. When the curing pressure was high (1.5 MPa, 2.0 MPa), most of the inner water was precipitated out because the strength of the specimen had a low setting time. The specimen volume decreased at the beginning of the final setting before gradually increased as well as continued to grow.

The final expansion ratios of the specimens were 4.7%, 1.36%, 0.62%, 0.45%, and 0.28% when the curing pressures were 0 MPa, 0.5 MPa, 1.0 MPa, 1.5 MPa, and 2.0 MPa, respectively. Under different curing pressure conditions, the functional relationship between the final expansion ratio ρ and the curing pressure P (Fig. 4(b)) is expressed as

$$\rho = 4.71 - 2 \times 2.257^{\left(1-e^{\frac{P}{0.503}}\right)}, \quad R^2 = 0.978 \tag{3}$$

4. Mechanical properties

4.1 UCS

Fig. 5 shows the UCS of the specimens with different expansion agent contents and curing pressure conditions.

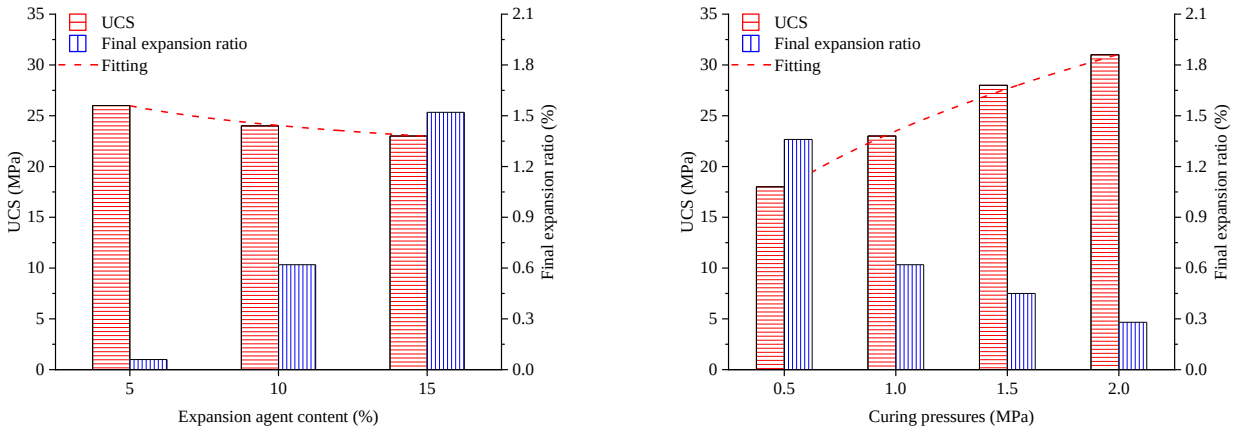

Fig. 5 UCS of specimens under different conditions, (a) Different expansion agent contents (1.0 MPa) and (b) Different curing pressures (10%)

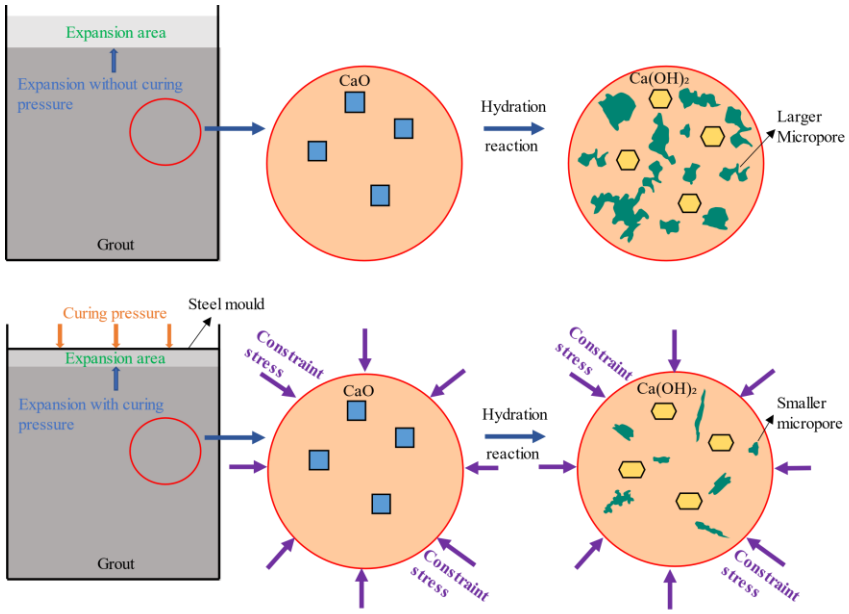

Fig. 6 Mechanisms of UCS of grout affected by curing pressure

4.1.1 Different expansion agent contents

It can be observed in Fig. 5(a) that under the same curing pressure condition (1.0 MPa), the UCS of the specimen decreased with an increase in the expansion agent content. The strength of the groups with 5%, 10%, and 15% expansion agent content reached 26.57 MPa, 24.40 MPa, and 23.37 MPa, respectively. The was slight changes in the strength under a 1.0 MPa curing pressure, and the expansion ratio reached 0.06%, 0.62%, and 1.52%, respectively. The results show that under the same curing pressure and different expansion agent contents, the was slight changes in the strength, but the expansion ratio changed greatly, which means the curing pressure greatly influenced the strength of the expansive grout. With different expansion agent contents, the functional relationship between the UCS(σ_c) and the expansion agent content φ (Fig. 5(a)) is expressed as

$$\sigma_c = 31.13\varphi^{-0.11}, \quad R^2 = 0.997 \tag{4}$$

4.1.2 Different curing pressures

As shown in Fig. 5(b), with the same expansion agent content (10%), the UCS of the specimen increased with increasing curing pressure. When the curing pressures were 0.5 MPa, 1.0 MPa, 1.5 MPa, and 2.0 MPa, the strengths were 18.2 MPa, 23.40 MPa, 27.97 MPa, and 31.51 MPa, and the expansion ratios were 1.36%, 0.62%, 0.45%, and 0.28%, respectively. The results show that under the same expansion agent content and different curing pressures, the strength and expansion ratio changed greatly, which means the curing pressure also greatly influenced the expansion ratio of expansive grout. Under different curing pressure conditions, the functional relationship between the UCS(σ_c) and the curing pressure P (Fig. 5(b)) is expressed as

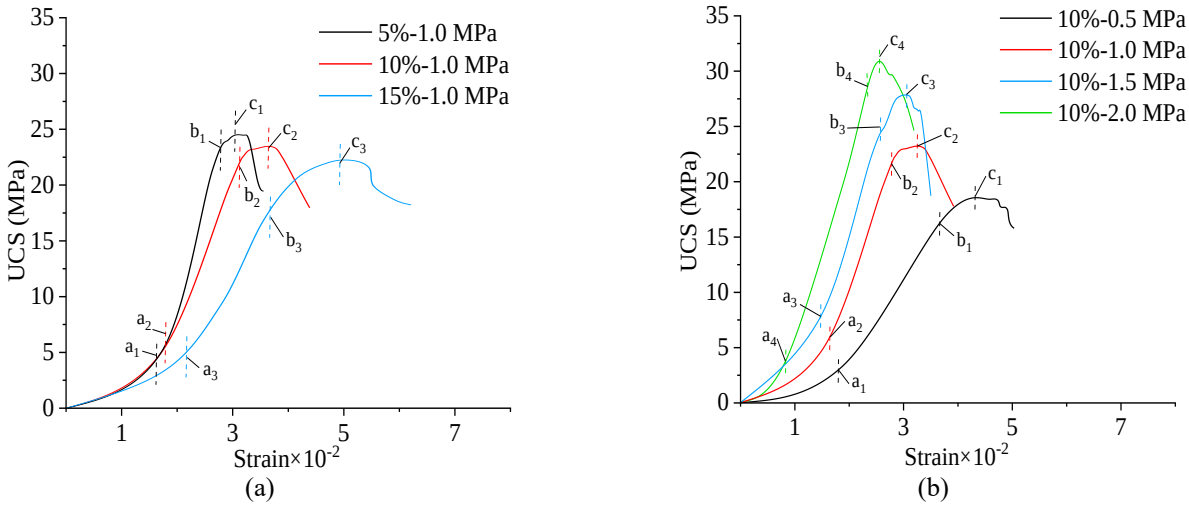

Fig. 7 UCS of specimens under different conditions, (a) Different expansion agent contents (1.0 MPa) and (b) Different curing pressures (10%)

$$\sigma_c = 23.49P^{0.41}, \quad R^2 = 0.998 \tag{5}$$

During expansion, the volume of the grout was restrained by the mold and the external curing pressure, increasing the interior compactness and the UCS of the expansive grout.

When the expansive grout was not cured under pressure and free to expand, the hydration reaction and the volume of the physical phase of CaO increased, which made the distance between the compounds to increase thus, macroscopically manifesting as an increase in the overall micropores of the grout, and a lower degree of the compactness, resulting in a decrease in its UCS. Also, when the expansive grout was cured under pressure, the external curing pressure caused a decrease in the pores, which improves the degree of the compactness and increases its UCS. The mechanism diagram is shown in Fig. 6.

4.2 Stress-strain curves

The stress–strain curves of the specimens with different expansion agent contents and curing pressures are shown in Fig. 7.

For all the specimens, the uniaxial compression was experienced through the initial pore–fissure compaction, elastic deformation, yield, and post–peak failure phases. The characteristics of each phase were different with different expansion agent contents and curing pressures, as shown in Fig. 7.

4.2.1 Different expansion agent contents

With increasing expansion agent content, the strain increased in the pore–fissure compaction and in the elastic deformation phases, the resistance to deformation weakened, the yield phase was prolonged, and the post-peak stress decreased slowly (Fig. 7(a)).

Pore–fissure compaction phase (o–a): When the expansion agent content was low (5%), the specimen's strain increased slowly under axial load, but the stress increased continuously, and the initial pore compaction phase demonstrated a convex curve. When the expansion agent content was high (15%), the compactness of the grout was relatively poor; under axial load, the strain of the specimen increased, but the change in stress slowed down.

Elastic deformation phase (a–b): The expansion agent content significantly affected the linear elastic phase of the compression process. When the expansion agent content was low, the strain of the linear elastic phase was small, and the resistance to deformation increased.

Yield phase (b–c): The yield phase of the specimen gradually lengthened with an increase in the expansion agent content, and the specimen changed from brittle to ductility.

Post–peak failure phase (c–): When the expansion agent content was low (5%), the stress decreased rapidly, and the strain increased slowly after the specimen was pressed to the peak strength, indicating strong brittleness. With an increase in the expansion agent content (15%), the specimen had a specific bearing capacity after the peak strength, and the stress decreased slowly.

4.2.2 Different curing pressures

With an increase in the curing pressure, in the pore–fissure compaction phase, the strain decreased as well as an increase in the stress. The strain was reduced in the elastic deformation phase, resistance to deformation increased, the yield phase shortened, and the post-peak stress decreased at a faster rate (Fig. 7(b)).

Pore–fissure compaction phase (o–a): The specimen exhibited a downward convex curve under axial load. With an increase in the curing pressure, the compactness of the specimen increased, the strain decreased, and the stress changes increased (Lu *et al*. 2020).

Elastic deformation phase (a–b): With an increase in the curing pressure, the specimen's strain decreased, and deformation resistance increased.

Yield phase (b–c): The yield phase shortened with an increase in curing pressure.

Post–peak failure phase (c–): When the curing pressure was low (0.5 MPa), the specimen had a specific bearing capacity after the peak strength. With an increase in curing

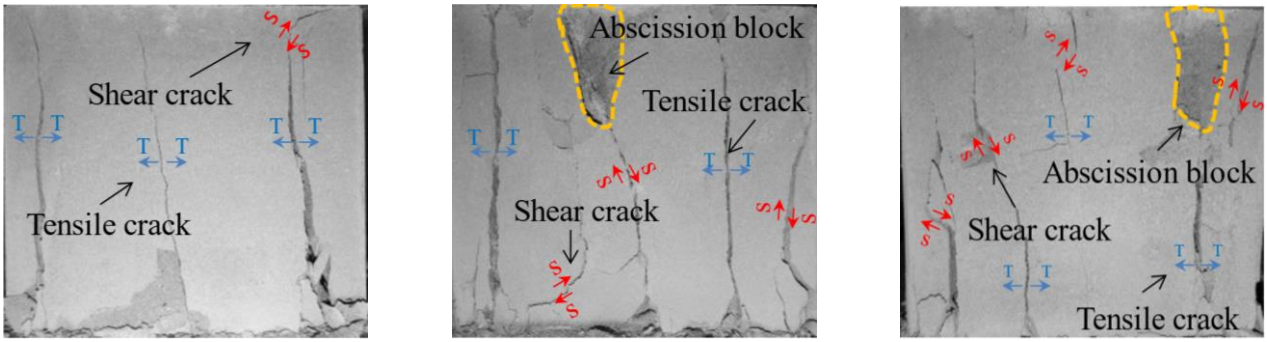

(a) (b) (c)

Fig. 8 Failure characteristics with different expansion agent contents (1.0 MPa), (a) 5%, (b) 10% and (c) 15%

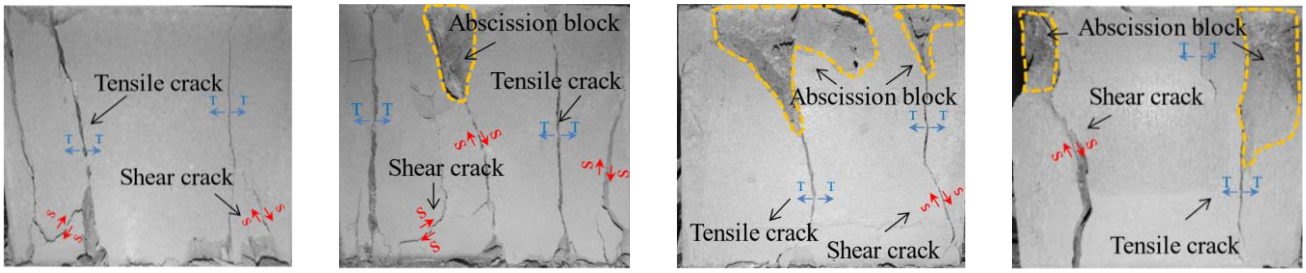

(a) (b) (c) (d)

Fig. 9 Failure characteristics with different curing pressures (10%), (a)0.5MPa, (b) 1.0 MPa, (c) 1.5 MPa and (d) 2.0 MPa

pressure, the degree of compactness increased, the bearing capacity decreased more rapidly, and the brittleness became more apparent.

4.3 Failure characteristics

The compression failure characteristics of the specimen after the uniaxial compression test are shown in Figs. 8 and 9. The typical failure modes of the grout were analyzed based on the expansion agent content and curing pressure.

4.3.1 Different expansion agent contents

With an increase in the expansion agent content, the failure mode changed from tensile failure to shear failure which increased the shear cracks and the main crack was gradually bent at an angle, as shown in Fig. 8.

Under the 1.0 MPa curing pressure, when the expansion agent content was low (5%), tensile cracks and a small number of shear cracks appeared under an axial load. Some of the tensile cracks run through the specimen, these were approximately axially parallel, and a small area of brittle chip cracking appeared on some end faces (Fig. 8(a)). When the expansion agent content was moderate (10%), the failure modes were tensile stress and shear stress, the shear cracks increased and flake cracks appeared (Fig. 8(b)). When the expansion agent content was high (15%), the failure of the specimen was caused by an axial tensile main crack, which appeared to bend at an angle and had a secondary crack (Fig. 8(c)).

4.3.2 Different curing pressures

With an increase in the curing pressure, the compactness of the specimen increased, the degree of chip cracking increased, and the brittle failure characteristics became more obvious after compression failure, as shown in Fig. 9.

With the 10% expansion agent content, when the curing pressure was low (0.5 MPa), tensile cracks and few shear cracks appeared in the specimen under axial load (Fig. 9(a)) (Zhang *et al*. 2021). When the curing pressure was moderate (1.0 MPa), the degree of chip cracking increased, tensile failure was dominant, and the brittle failure was more obvious (Fig. 9(b)). When the curing pressure was high (1.5 MPa, 2.0 MPa), the cracking of the specimen was more severe, and the integrity of the specimen decreased after failure (Figs. 9(c) and 9(d)).

5. Microevolutionary analysis

With different expansion agent contents and curing pressures, the expansive grout's macro expansion properties and mechanical properties were analyzed through XRD patterns, SEM images, and surface morphology characteristics.

5.1 XRD patterns

Fig. 10 shows the XRD patterns of the specimens with different expansion agent contents and curing pressures. The structure of the diffraction patterns was similar, indicating that the styles of hydration products of the expansive grout were essentially stable after the final setting and were not affected by the curing pressures. The main characteristic peaks were the main hydration products, C-S-H and $Ca(OH)_2$, their positions were essentially the same. The peak area of C-S-H was the largest, and the other peaks corresponded to ettringite (Aft) and a small amount of dicalcium silicate (C_2S).

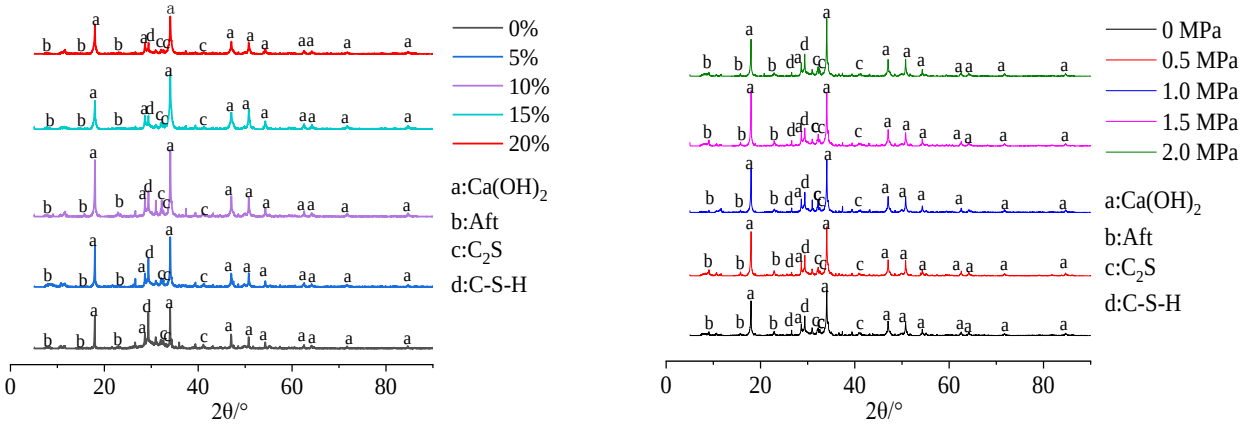

Fig. 10 XRD patterns under different conditions, (a) Different expansion agent contents (1.0 MPa) and (b) Different curing pressures (10%)

(i) The diffraction peak areas of $Ca(OH)_2$ and C-S-H increased with an increase in the expansion agent content (Fig. 10(a)), and the relative difference between the peak areas of $Ca(OH)_2$ and C-S-H gradually decreased, indicating a gradual increase in $Ca(OH)_2$ content.

(ii) The peak areas of $Ca(OH)_2$ and C-S-H decreased with increasing curing pressure (Fig. 10(b)), indicating the reduction in hydration products and the degree of hydration.

5.2 SEM images

Figs. 11 and 12 show SEM images of specimens with different expansion agent contents and curing pressures.

5.2.1 Different expansion agent contents

With an increase in the expansion agent content, the content of $Ca(OH)_2$ increased, and the specimen volume increased. $Ca(OH)_2$ had low strength and was extruded by C-S-H with higher strength (Ylmén *et al.* 2009, Double *et al.* 1978), there were many pores in the specimen due to extrusion and irregular crystal morphology, which weakened the strength of the specimen.

(i) When the expansion agent content was 0% (Fig. 11(a)), the absolute quantity of hydration products was relatively small. The specimen mainly contains floc-like C-S-H gels, hexagonal $Ca(OH)_2$ crystals, and needle-like AFt crystals (Colombo *et al.* 2018). After solidification, there were more capillary voids in the specimen and less contact between the crystals. Macroscopically, the grout volume decreased somewhat after solidification due to less water consumed by hydration and more significant drying shrinkage.

(ii) When the expansion agent content was 5% (Fig. 11(b)), the amount of water consumed by hydration increased, the absolute amount of hydration products increased, and the dry shrinkage decreased owing to the CaO in the expansion agent. The $Ca(OH)_2$ crystals expanded and gradually filled the pores between the crystals, increasing the resistance to dry shrinkage. Macroscopically, the specimen slightly expanded.

(iii) When the content of the expansion agent was 10% or 15% (Figs. 11(c) and 11(d)), a large amount of CaO engaged in the hydration reaction and produced hydration products. $Ca(OH)_2$ crystals continued to grow and increase, with a particular strength of C-S-H, making extrusion that resulted in excessive expansion stress, destroying the internal structure, producing pores, and reducing the degree of compactness. Macroscopically, the specimen greatly expanded, but the strength was reduced.

(iv) When the expansion agent content was 20% (Fig. 11(e)), the hydration products further increased. There were many pores in the specimen due to extrusion between the C-S-H gels and $Ca(OH)_2$ crystals, the crystals became irregular. Macroscopically, the specimen expanded further, but the strength was lower.

5.2.2 Different curing pressures

With an increase in the curing pressure, the pores in the specimen decreased, and the growth of $Ca(OH)_2$ was limited, the volume expansion of the specimens decreased. The higher curing pressure increased the compactness of the specimen, as well as its strength.

(i) When the curing pressure was not applied (Fig. 12(a)), there were more pores between the crystals, and the hydration reaction was more complete. The growth of $Ca(OH)_2$ was not limited by the curing pressure, the content of $Ca(OH)_2$ was high, and the specimens had large volume expansion. The specimens had many pores, and the compactness was low under no curing pressure.

(ii) When the curing pressure was 0.5 MPa (Fig. 12(b)), compression between the crystals resulted in a reduction in pore water and capillary water, and a subsequent decrease in hydration products. Macroscopically, the volume expansion ratio of the entire specimen was much smaller than without curing pressure.

(iii) As the curing pressure increased to 1.0 MPa or 1.5 MPa (Figs. 12(c) and 12(d)), there were fewer pores between crystals, the specimen compactness increased, and the hydration process was further hindered. When the curing pressure was 2.0 MPa (Fig. 12(e)), because C-S-H gels were stronger than $Ca(OH)_2$ crystals, further crushing of $Ca(OH)_2$ crystals occurs through extrusion. Macroscopically, the volume expansion of the entire specimen continued to decrease, and the strength was higher.

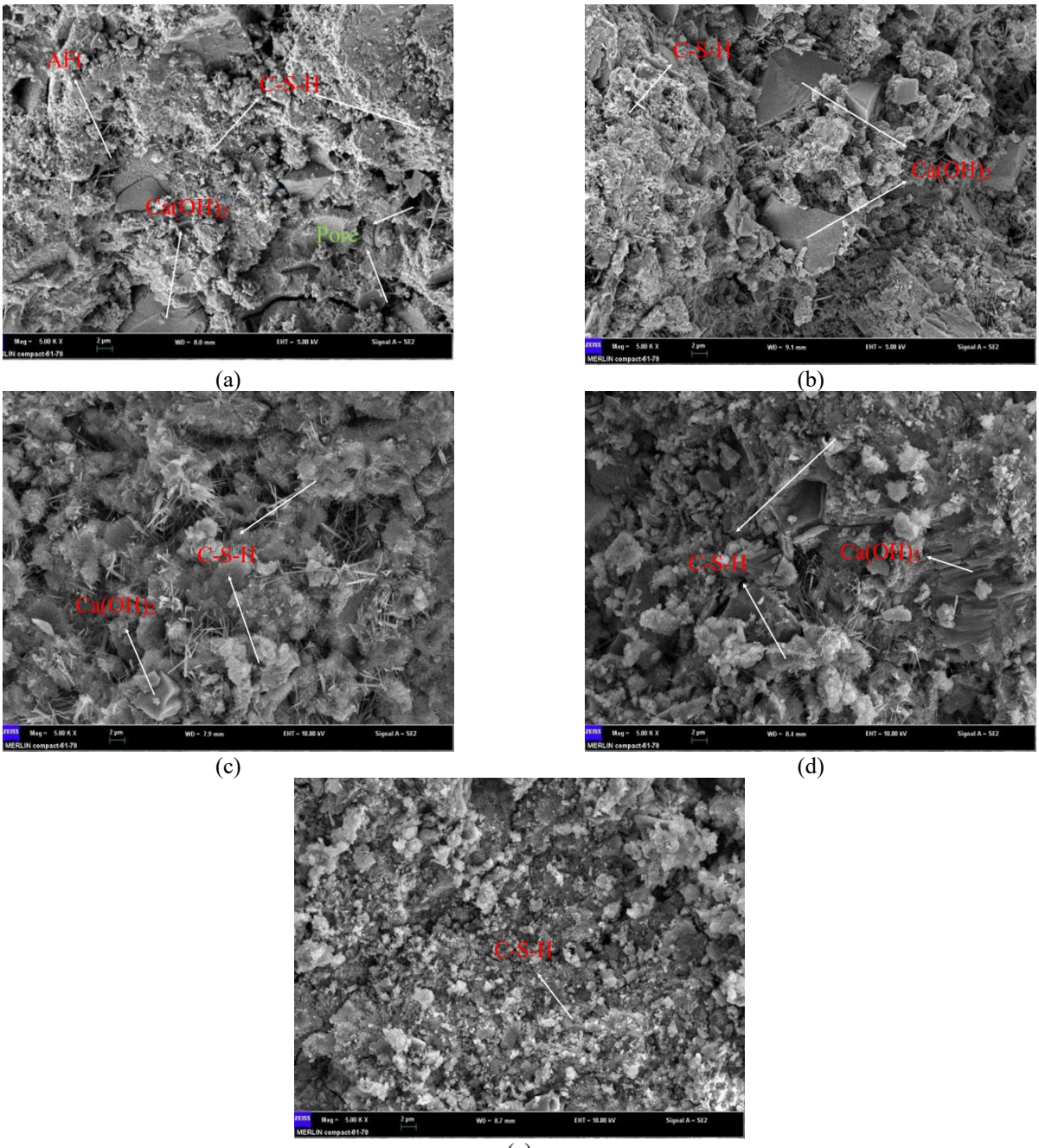

Fig. 12 SEM images of different curing pressures, (a) 10%-0 MPa, (b) 10%-0.5 MPa, (c) 10%-1.0 MPa, (d) 10%-1.5 MPa and (e) 10%-2.0 MPa

5.3 Microscopic scanning images

Figs. 13 and 14 show cross-sections at the center of specimens with different expansion agent contents and curing pressures at 200 × magnification using a microscope scanner, three positions were randomly selected for each specimen. The concave surface proportion, represented in green, was calculated using MATLAB based on the surface morphology results.

The results show that the proportion of concave surfaces in the specimen center's cross-section reflected the specimen's porosity to a certain extent. The proportion of the concave surface was linear with increasing expansion agent content and curing pressure. It was consistent with the results of the SEM. The higher the porosity, the lower the compactness, and the higher strength, which was consistent with the strength variation law of the expansive grout specimens.

5.3.1 Different expansion agent contents

It is observed in Fig. 13 that under the 1.0 MPa curing pressure, the proportion of the concave surface increased gradually with an increase in the expansion agent content, indicating an increasing number of pores produced from extrusion between $Ca(OH)_2$ crystals and C-S-H. Thus, the

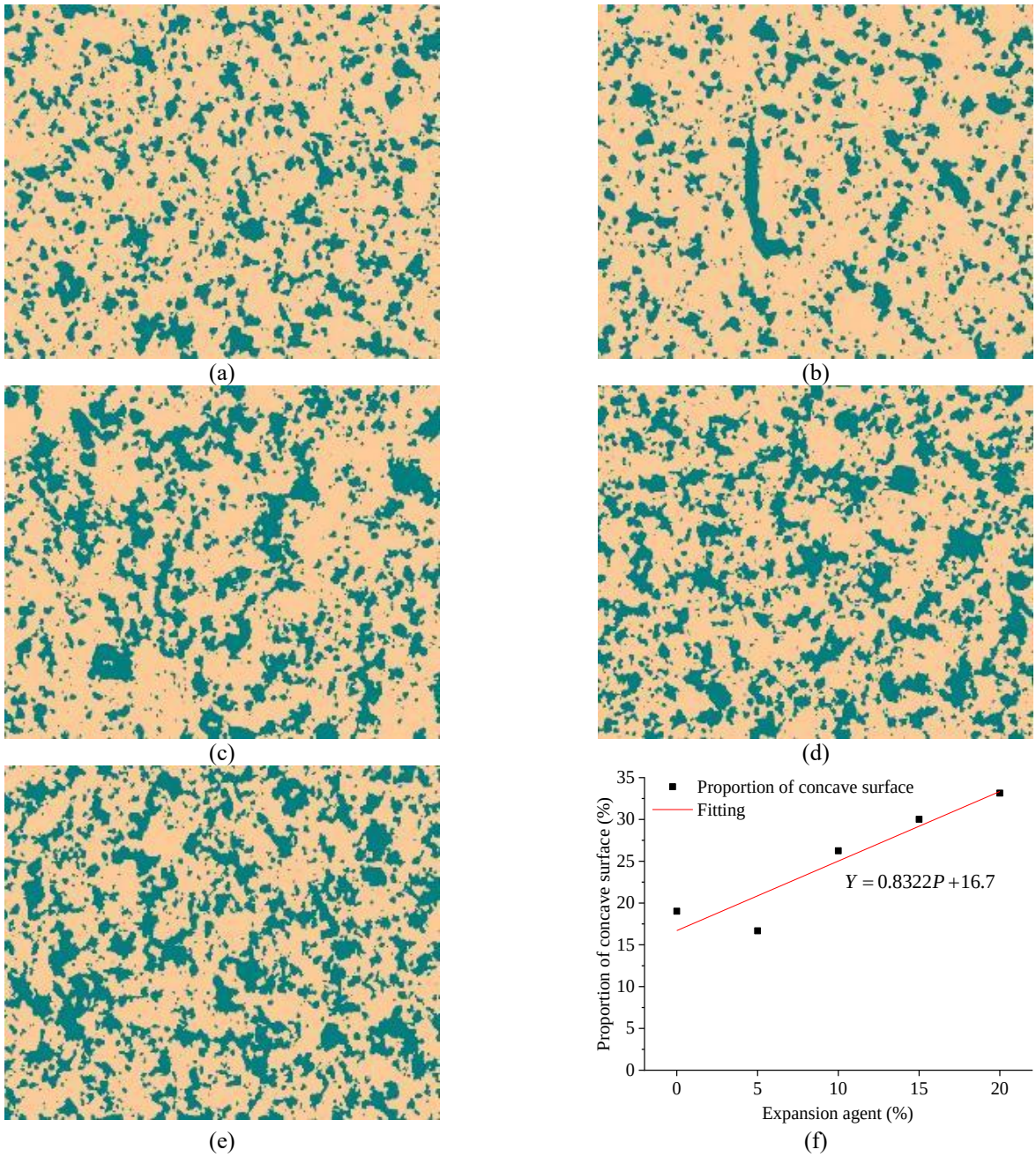

Fig. 13 Surface morphology of specimens with different expansion agent contents (1.0 MPa), (a) 10%-0 MPa, (b) 10%-0.5 MPa, (c) 10%-1.0 MPa, (d) 10%-1.5 MPa, (e) 10%-2.0 MPa and (f) Proportion of concave surfaces with different expansion agent contents

degree of compactness was further reduced which decreased the specimen strength.

The proportions of the concave surfaces were 19.02%, 16.67%, 26.25%, 30.02%, and 33.15%, with 0%, 5%, 10%, 15%, and 20% expansion agent content, respectively. It can be noted that the concave surface proportion decreased when the expansion agent content was 5%. The functional relationship between the proportion of concave surfaces Y and expansion agent content φ is shown in Fig. 13(f); the proportion of concave surfaces of the specimen was linear with the expansion agent content.

5.3.2 Different curing pressures

It can be observed in Fig. 14 that with the 10% expansion agent content, the proportion of the concave surfaces decreased gradually with an increase in curing pressure, indicating an increase in the number of pores, occurrence of extrusion under axial load, and a decrease in the pore water and capillary water hindering the hydration reaction. The pores were further compressed, which resulted in a higher degree of compactness and an increased in strength, and the brittle failure characteristics became more obvious.

The proportion of the concave surfaces was 34.59%, 28.34%, 26.25%, 23.4%, and 20.63% under curing pressures of 0 MPa, 0.5 MPa, 1.0 MPa, 1.5 MPa, and 2.0 MPa, respectively. The functional relationship between the

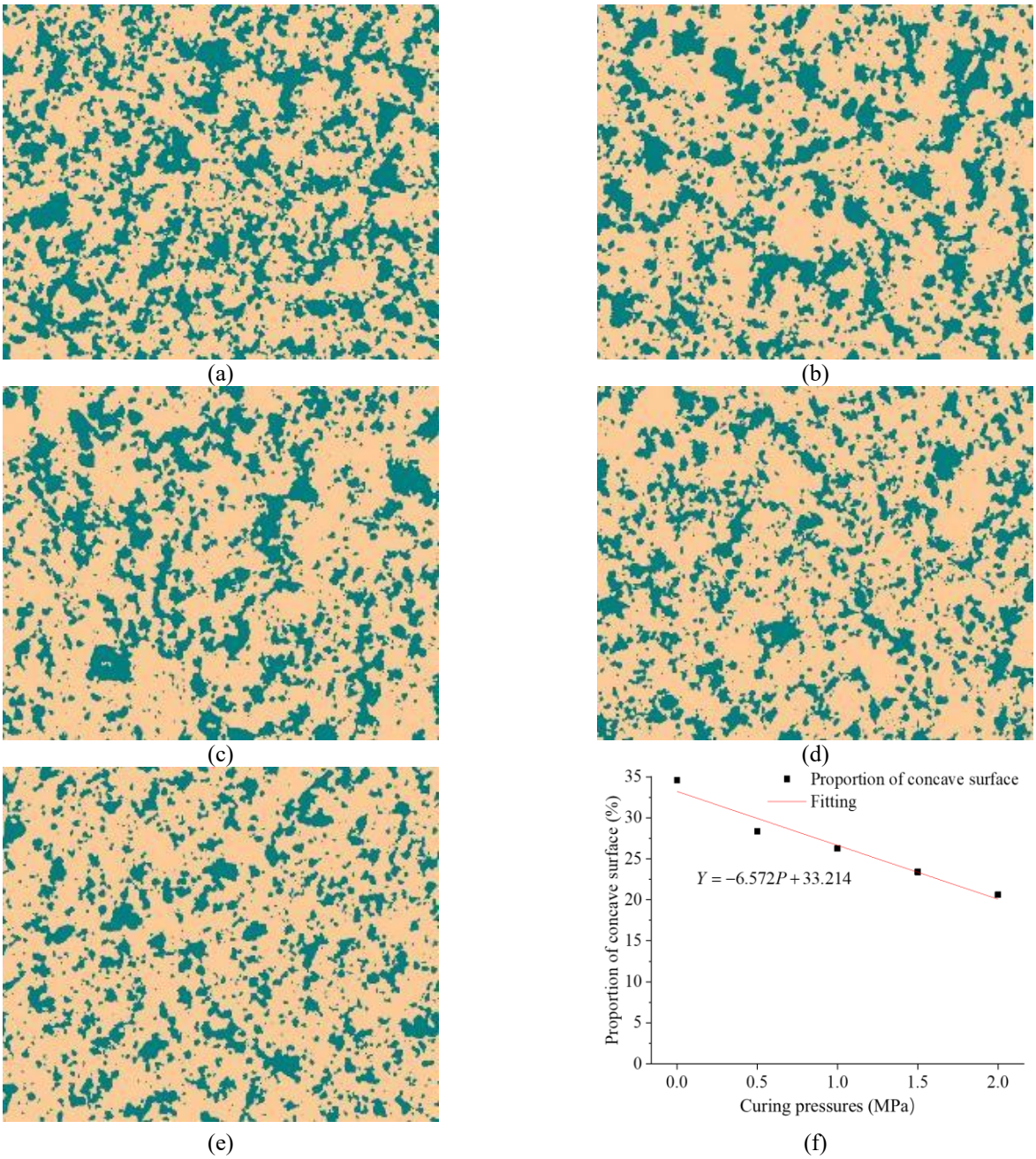

Fig. 14 Surface morphology of specimens with different curing pressures, (a) 10%-0 MPa, (b) 10%-0.5 MPa, (c) 10%-1.0 MPa, (d) 10%-1.5 MPa, (e) 10%-2.0 MPa and (f) Proportion of concave surfaces with different curing pressures

proportion of the concave surfaces Y of the specimens and the change in the curing pressure P is shown in Fig. 14(f), indicating that the proportion of the concave surfaces of the specimen was linear with the curing pressure.

With an increase in the expansion agent content, the expansion ratio of the expansive grout increased with a decrease in the strength. The results interpreted at the microscopic level are as follows, expansion agent directly affected the hydration process and produced more $Ca(OH)_2$ crystals, more pores occurred in the specimen due to extrusion between the crystals, and the degree of compactness became lower.

With an increase in the curing pressure, the expansion ratio of the expansive grout decreased with an increase in the strength. The results interpreted at the microscopic level are as follows, the curing pressure directly increased the compactness of the expansive grout. There were fewer pores between the crystals, and the water required for $Ca(OH)_2$ crystal volume growth was less, further hindering the hydration process which resulted in less production of $Ca(OH)_2$ crystals.

6. Conclusions

Considering the expansive grout with HCSA as an expansion source, the expansion performance and mechanical properties under different curing pressure conditions were analyzed using the expansion ratio tests,

UCS tests, XRD, SEM, and MSTs. At the macro and micro levels, the influencing factors of expansion performance and mechanical strength were analyzed based on the experimental results. From this study, the following conclusions can be drawn:

(1) The final expansion ratio of the expansive grout was linear with an increase in expansion agent content and nonlinear with an increase in curing pressure. The expansion effect was related mainly to the development of $Ca(OH)_2$ crystals thus, a higher expansion agent content produced more $Ca(OH)_2$ crystals. As the curing pressure increased, the number of pores between the crystals decreased, and the compactness of the grout increased, hindering the hydration process of the $Ca(OH)_2$ crystals' generation as well as reducing the water content.

(2) The strength of the expansive grout was negatively correlated with the expansion agent content and positively related to curing pressure. More $Ca(OH)_2$ crystals were formed with an increase in the expansion agent content. They were extruded with C-S-H at a certain strength, resulting in excessive expansion stress, destruction of the internal structure, and reduced compactness. Thus, the strength of the expansive grout was reduced. With an increase in the curing pressure, the internal pores were compressed, and the compactness of the grout increased significantly which increased the strength of the grout.

(3) With an increase in the expansion agent content, the compactness of the grout decreased, and there were more pores. The failure mode of the grout changed: tensile failure was dominant, and shear failure occurred locally. With an increase in the curing pressure, the grout became more compact, the fracture degree increased, and the brittle failure characteristics became more obvious.

Acknowledgments

This study was supported by the National Natural Science Foundation of China (Grant No. 51804224) and the Key Research and Development Plan of Hubei Province (No. 2020BCA082), and the Graduate Innovation and Entrepreneurship Fund of Wuhan University of Science and Technology (No. JCX201858). We would like to thank Elsevier Language Editing Services for English language editing.

References

Colombo, A., Geiker, M., Justnes, H., Lauten, R.A. and De Weerdt, K. (2018), "The effect of calcium lignosulfonate on ettringite formation in cement paste", *Cement Concrete Res*., **107**(2018), 188-205. https://doi.org/10.1016/j.cemconres.2018.02.021.

Das, R. and Singh, T.N. (2020), "Effect of rock bolt support mechanism on tunnel deformation in jointed rockmass: A numerical approach", *Undergr. Space*, **6**(4), 409-420. https://doi.org/10.1016/j.undsp.2020.06.001.

De Silva, V.R.S., Ranjith, P.G., Perer, M.S.A., Wu, B. Rathnaweera, T.D. (2017), "Investigation of the mechanical, microstructural and mineralogical morphology of soundless cracking demolition agents during the hydration process", *Mater. Characterization* **130**, 9-24. https://doi.org/10.1016/j.matchar.2017.05.004.

De Silva, V.R.S., Ranjith, P.G., Perer, M.S.A. and Wu, B. (2019), "The effect of saturation conditions on fracture performance of different soundless cracking demolition agents (SCDAs) in geological reservoir rock formations", *J. Nat. Gas Sci. Eng*., **62**, 157-170. https://doi.org/10.1016/j.jngse.2018.11.013.

Double, D.D., Hellawell, A. and Perry, S.J. (1978), "The hydration of Portland cement", *Proceedings of the Royal Society A: Mathematical, Physical and Engineering Sciences*, **261**(1699), 486-488. https://doi.org/10.1038/261486a0.

EI Tani, M. (2012), "Grouting rock fractures with cement grout", *Rock Mech. Rock Eng.*, **45**(4), 547-561. https://doi.org/10.1007/s00603-012-0235-0.

Huang, K.J., Shi, X.J., Zollinger, D., Mirsayar, M., Wang, A. and Mo, L.W. (2019), "Use of MgO expansion agent to compensate concrete shrinkage in jointed reinforced concrete pavement under high-altitude environmental conditions", *Constr. Build. Mater.*, **202**, 528-536. https://doi.org/10.1016/j.conbuildmat.2019.01.041.

Laefer Debra, F., Natanzi Atteyeh, S. and Iman Zolanvari, S.M. (2018), "Impact of thermal transfer on hydration heat of a Soundless Chemical Demolition Agent", *Constr. Build. Mater.*, 187. 348-359. https://doi.org/10.1016/j.conbuildmat.2018.07.168.

Lai, M.H., Binhowimal, S., Griffith, A.M., Hanzic, L. and Ho, J. (2020), "Shrinkage, cementitious paste volume, and wet packing density of concrete", *Struct. Concrete*, 10. https://doi.org/10.1002/suco.202000407

Li, Z.P., Zhang, L.Z., Chu, Y.T. and Zhang, Q.S. (2020), "Research on influence of water-cement ratio on reinforcement effect for permeation grouting in sand layer", *Adv. Mater. Sci. Eng.*, **1**, 1-12. https://doi.org/10.1155/2020/5329627.

Liu, C.W. and Lu, S.L. (2000), "Reinforcement effect of cement grouting on engineering rock mass", *J. China Univ. Mining & Technology*, **29**(5), 454-458. https://doi.org/10.3321/j.issn:1000-1964.2000.05.003.

Liu, S.W., He, Y. and Fu, M.X. (2020), "Experimental investigation of surrounding-rock anchoring synergistic component for bolt support in tunnels", *Tunn. Undergr. Sp. Technol.*, **104**(12), 103531. https://doi.org/10.1016/j.tust.2020.103531.

Lu, J., Yin, J.Z., Zhang, D.M., Gao, H., Li, C.B. and Li, M.H. (2020), "True triaxial strength and failure characteristics of cubic coal and sandstone under different loading paths", *Int. J. Rock Mech. Min. Sci.*, **135**(11), 104439. https://doi.org/10.1016/j.ijrmms.2020.104439.

Moayed, R.Z., Hosseinali, M., Shirkhorshidi, S.M. and Sheibani, J. (2019), "Experimental investigation and constitutive modeling of grout-sand interface", *Int. J. Geomech*., **19**(5), 04019024.1-04019024.13. https://doi.org/10.1061/(ASCE)GM.1943-5622.0001384.

Natanzi Atteyeh, S., Laefer Debra, F. and Iman Zolanvari, S.M. (2020), "Selective demolition of masonry unit walls with a soundless chemical demolition agent", *Constr. Build. Mater*., **248**, 118635. https://doi.org/10.1016/j.conbuildmat.2020.118635.

Pedrotti, M., Wong, C., El Mountassir, G. and Lunn, R.J. (2017), "An analytical model for the control of silica grout penetration in natural groundwater systems", *Tunn. Undergr. Sp. Technol.*, **7**, 105-113. https://doi.org/10.1016/j.tust.2017.06.023.

Saeidi, O., Stille, H. and Torabi, S.R. (2013), "Numerical and analytical analyses of the effects of different joint and grout properties on the rock mass groutability", *Tunn. Undergr. Sp. Technol*., **38**, 11-25. https://doi.org/10.1016/j.tust.2013.05.005.

Shang, J., West, L.J., Hencher, S.R. and Zhao, Z. (2018a), "Tensile strength of large-scale incipient rock joints: a laboratory

investigation", *Acta Geotechnica*, **13**(4), 869-886. https://doi.org/10.1007/s11440-017-0620-7.

Shang, J., Zhao, Z. and Aliyu, M.M. (2018b), "Stresses induced by a demolition agent in nonexplosive rock fracturing", *Int. J. Rock Mech. Min. Sci*., **107**, 172-180. https://doi.org/10.1016/j.ijrmms.2018.04.049.

Shimada, H., Hamanaka, A., Sasaoka, T. and Matsui, K. (2014), "Behaviour of grouting material used for floor reinforcement in underground mines", *Int. J. Min. Reclamation Environ*., **28**(2), 133-148. https://doi.org/10.13722/j.cnki.jrme.2016.0934.

Varol, A. and Dalg, S. (2006), "Grouting applications in the Istanbul metro, Turkey", *Tunn. Undergr. Sp. Technol.*, **21**(6), 602-612. https://doi.org/10.1016/j.tust.2005.11.002.

Wang, P.X., Zhang, X.D., Zhang, B., Jiang, L.Z. and Xie, M.W. (2014), "Effect of the expansion agent on early-age autogenous shrinkage stress of concrete", *Adv. Mater. Res*., **838-841**, 564-568. https://doi.org/10.4028/www.scientific.net/AMR.838-841.564.

Wang, Q., Qin, Q., Jiang, B., Yu, H.C., Pan, R. and Li, S.C. (2019), "Study and engineering application on the bolt-grouting reinforcement effect in underground engineering with fractured surrounding rock", *Tunn. Undergr. Sp. Technol.*, **84**, 237-247. https://doi.org/10.1016/j.tust.2018.11.028.

Widmann, R. (1996), "International society for rock mechanics commission on rock grouting", *Int. J. Rock Mech. Min. Sci. Geomech. Abstracts*, **33**(8), 803-847. https://doi.org/10.1016/S0148-9062(96)00015-0.

Yao, N., Chen, J.W., Hu, N.Y., Ye, Y.C., Xiao, Y.H. and Huang, Y. (2021), "Experimental study on expansion mechanism and characteristics of expansive grout", *Constr. Build. Mater*., **268**, 121574. https://doi.org/10.1016/j.conbuildmat.2020.121574.

Ylmén, R., Jäglid, U., Steenari, B.M. and Panas, I. (2009), "Early hydration and setting of Portland cement monitored by IR, SEM and Vicat techniques", *Constr. Build. Mater*., **39**(5), 433-439. https://doi.org/10.1016/j.cemconres.2009.01.017.

Zhang, J.P., Liu, L.M., Li, Q.H., Peng, W., Zhang, F.T., Cao, J.Z. and Wang, H. (2019), "Development of cement-based self-stress composite grouting material for reinforcing rock mass and engineering application", *Constr. Build. Mater.*, **201**, 314-327. https://doi.org/10.1016/j.conbuildmat.2018.12.143.

Zhang, S.C., Li, Y.Y., Liu, H. and Ma, X.W. (2021), "Experimental investigation of crack propagation behavior and failure characteristics of cement infilled rock", *Constr. Build. Mater.*, **268**, 121735. https://doi.org/10.1016/j.conbuildmat.2020.121735.

Zhang, X., Wang, M.N. and Wang, Z.L. (2020), "Stability analysis model for a tunnel face reinforced with bolts and an umbrella arch in cohesive-frictional soils", *Comput. Geotech*., **124**(2-3), 103635. https://doi.org/10.1016/j.compgeo.2020.103635.

Zhi, W., Li, L., Guo, S.C., Dai, Q.L. and Qing, L. (2018), "Nonlinear fatigue damage of cracked cement paste after grouting enhancement", *Appl. Sci*., **8**(7), 1105. https://doi.org/10.3390/app8071105.

CC